Experimental study of the wake flow behind three road vehicle models

R. RODRIGUEZ[a], F. MURZYN[a], A. MEHEL[b], F. LARRARTE[c]

a. Laboratoire de l'Ecole Supérieure des Techniques Aéronautiques et de Construction Automobile (ESTACA'Lab) - Ecole Supérieure des Techniques Aéronautiques et de Construction Automobile - Rue Georges Charpak, 53 000 Laval, France
romain.rodriguez@estaca.fr
b. Laboratoire de l'Ecole Supérieure des Techniques Aéronautiques et de Construction Automobile (ESTACA'Lab) - Ecole Supérieure des Techniques Aéronautiques et de Construction Automobile - 12 rue Paul Delouvrier - RD 10 78180 Montigny-le-Bretonneux, France
c. IFSTTAR/GERS/LEE – Centre de Nantes Route de Bouaye – CS 4 44344 Bouguenais Cedex, France

Abstract :

Wind tunnel investigations have been conducted in the wake of three simplified car models, commonly called Ahmed body, with 0°, 25° and 35° rear slant angle respectively. The upstream velocity is 14.3m/s, leading to a Reynolds number based on the model height of 4.95×10^4. *Velocity measurements have been recorded with a Laser Doppler Velocimetry system. An innovative data treatment method has been developed to obtain accurate and reliable flow statistics regardless the seeding conditions. Wake flow properties such as the recirculation length, turbulence intensity or turbulent kinetic energy are similar to results found in the literature. Further works will consist in measuring the nanoparticle concentration fields in the wake of the same models, in order to better understand the particle dynamics and especially the interaction between turbulent vortical structures and particles. The final goal of the project is to identify key parameters that influence particle path and possible infiltration in the following vehicle through air entrances.*

Mots clefs : Wind tunnel, Wake flow, LDV, data analysis, Ahmed body

1 Introduction

The increasing exposure of car passengers, cyclists and pedestrians to air pollution has become a major concern for the sanitary authorities, inducing great interest from the scientific community. Pollutants (gaseous and solid particles) are emitted by different sources and it is worthwhile to note that ground vehicles are one of the main contributors to their high concentration levels in urban areas. Among them, UltraFine Particles (UFP) with diameter below 100nm and gas such as nitrogen oxides (NOx) are issued from engine combustion, meaning that there are key issues for automotive engineering. UFP may be inhaled by breathing and can penetrate into the respiratory system, having strong health impacts by increasing asthma exacerbations and risks of cardiovascular and pulmonary diseases. This is mainly due

to their small size making these particles able to penetrate deeper into the respiratory system. The World Health Organization (WHO) assesses the mortality for 53 European countries as 482 000 premature deaths per year and also associated sanitary costs of about 2.3% of Gross Domestic Product (GDP) in France.

Recent studies have shown that UFP concentrations may be larger inside the cabin than outside (Goel and Kumar [1]). Decreasing the infiltration rates and thus exposure of car passenger during commuting time is then a major goal. Having that in mind, understanding the nanoparticle dispersion in the wake of a car is paramount. Characterizing the interactions between particles and the surrounding flow (wake flow) would be an asset to improve our knowledge on the particle dynamics and their ability to infiltrate the car cabin. Although numerical studies and on road measurements are quite numerous (Goel and Kumar [1], Kumar et al. [2]), our interest is focused on experimental investigations of UFP distribution in the wake of a reduced scale model in wind tunnel. To achieve this goal, a first step is to provide an accurate description of the flow dynamics downstream of a car. This paper aims at addressing this key-issue according to a new data analysis method. This new method corrects possible bias that depends on the seeding conditions, ensuring the reliability and accuracy of statistical moments.

After this introduction and presentation of the challenges related to our project, the second part of the present paper is dedicated to the basic characteristics of the flow behind a simplified car model. In the third part, the instrumentation and experimental facilities are described. A special interest is dedicated to an innovative LDV (Laser Doppler Velocimetry) data analysis method that has been developed to avoid statistical bias. In the fourth part, the main significant results are presented for different rear slant angles and compared with the literature. Conclusions and future works are discussed in the last section.

2 Characteristics of the flow behind Ahmed body

Aerodynamics of road vehicles is often characterized through the drag force. This force can be divided into two terms related to friction and pressure. According to Hucho [3], frictional drag is predominant for streamlined profiles whereas pressure drag is the most contributing factor for road vehicles assimilated as bluff bodies. This is mostly explained by flow separations occurring at the vehicle front-end (front edge of the hood, in front of the windshield, exterior mirrors, wheels, ...) as well as at the after-body generating low pressure wake (Hucho [3]). For wake flow investigations, Ahmed et al. [4] proposed the so-called Ahmed body for which the rear slant angle is the sole varying parameter (Figure 1). Note that the length of the rear slant being fixed (222mm), so configurations with $\varphi = 0°$ and $\varphi = 90°$ are the same. This shape avoids flow separations from the front of the car model. Then, by changing the rear slant angle φ, the structure of wake flow differs as well as the drag representing most of situations arising behind real cars.

According to that model, different wake flow structures have to be considered depending on the rear slant angle (Ahmed et al. [4]):

- $\varphi < 12.5°$ (Figure 2(a)): the flow remains fully attached on the rear slant and the downwash effect is very strong. Two longitudinal vortices develop due to the enrolment of the boundary layer around the rear slant edges. In the near-wake, a system of horseshoe vortices is visible. They are counter-rotating if observed in the symmetry plane. For the squareback configuration ($\varphi = 0°$), it has been shown that the length of the recirculating region corresponds to approximately $1.5h$ (h

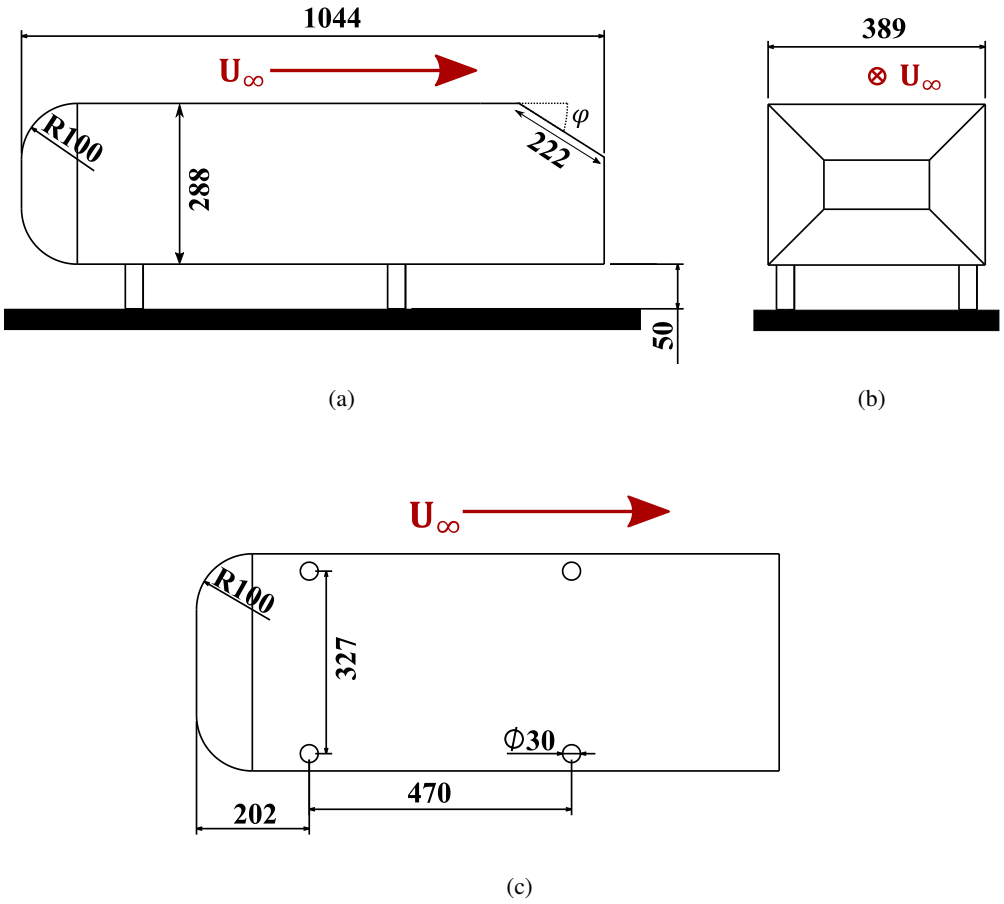

Figure 1: Schematic of the Ahmed body proposed by Ahmed et al. [4] (dimensions are in millimetres). The rear slant has a fixed length and its inclination φ is changing: (a) Side view, (b) Front view, (c) Bottom view

being the height of the model). Nevertheless, it can differ according to the experimental conditions (Lahaye [5]).

- $12.5° < \varphi < 30°$ (Figure 2(b)): the flow is partially separated from the rear slant. As a consequence of the separation bubble occurring on the rear slant, a higher vorticity is observed in the longitudinal vortices (Thacker [6]). In the near wake, the horseshoe vortices are still present. Therefore, interactions between all these structures lead a highly three-dimensional flow.

- $\varphi > 30°$: the flow is fully detached from the rear slant. As a result, the longitudinal vortices do not exist anymore since they are no more fed. Nevertheless, the flow structure is very close to that of $\varphi < 12.5°$.

To date, mean and fluctuating velocity fields in the wake of the car model have been widely studied either experimentally or numerically (Barros [7], Lahaye [5]). However, even if the flow structures described previously have always been identified, they are very sensitive to the experimental conditions, such as:

- Separation flow around the front edge that may exist and influence the turbulent wake fields of the Ahmed body (Spohn and Gilliéron [8]).

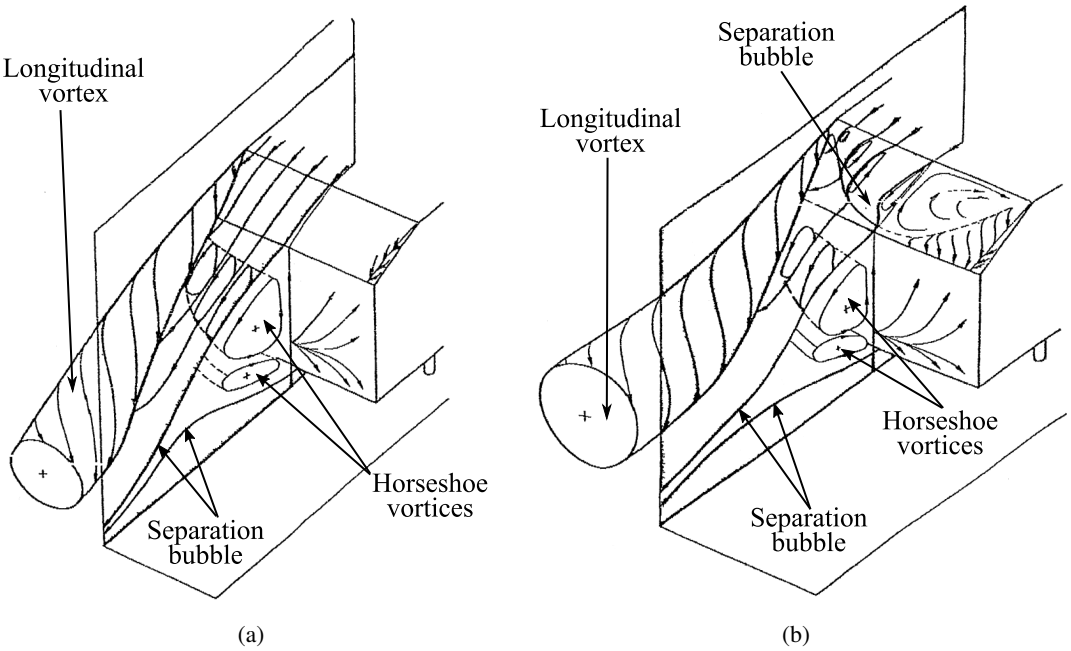

Figure 2: Schematic of flow structures in the wake of the Ahmed body according to the study of Ahmed et al. [4]: (a) $\varphi < 12.5°$, (b) $12.5° < \varphi < 30°$

- Presence of the rear slant separation bubble for $12.5° < \varphi < 30°$ that is not systematic since it is highly dependent on the sharpness of the edge between roof and slant (Thacker [6]).
- Height of the model stilts (Grandemange [9]) as well as the perturbation of the underbody flow (Barros [7]) which influence the properties of horseshoe vortices.

As a consequence, an accurate description of the mean and fluctuating velocity fields corresponding to our experimental conditions is required.

3 Experiments and data analyses techniques

3.1 Instrumentation and experimental set-up

The car models used in this study are 0.19 scaled Ahmed bodies with rear slant angles of 0°, 25° and 35° (Figure 3). The co-ordinate system (x, y, z) associated with the model is also presented, (X, Y, Z) are the associated dimensionless distances (the height h of the car model being the scaling length). (u, v, w) are the components of the velocity vector, $(\bar{u}, \bar{v}, \bar{w})$ and (u', v', w') being the corresponding time averaged and fluctuating (in Reynolds decomposition meaning) values, respectively.

Measurements were conducted in the open-circuit wind tunnel manufactured by DeltaLab (reference model EA103). The test section is 1m in length, 0.3m in both height and width. The maximum speed velocity is 40m/s. An important calibration campaign has been achieved to characterize the incoming flow in an empty test section. The main conclusions state that the maximum streamwise turbulence intensity u'/U_∞ was less than 1% (outside of the boundary layer) and that the boundary layer is turbulent with a maximum thickness of 12mm at the exit of the test section (partially-developed inflow conditions).

The model is fixed on the floor of the test section by a cylindrical rod (diameter 5mm) and four stilts are used which height and diameter are 15mm (noted h_s) and 6mm respectively. Note that their height is larger than the maximum boundary layer thickness. The relative ground clearance is $H_s = h_s/h = 0.28$. The blockage coefficient, defined as the ratio between the model frontal area and the test section area is below 5%. Then no correction is needed for the blockage effect (Wang et al. [10]). For experiments with particles, the ratio between velocities of the upstream flow and the exhaust gas one will be similar to that of a real car moving in an urban area. Then, a constant upstream velocity of $U_\infty = 14.3m/s$ is considered in the present paper. The Reynolds number based on the model height is $\mathcal{R}e_h = 4.95 \times 10^4$.

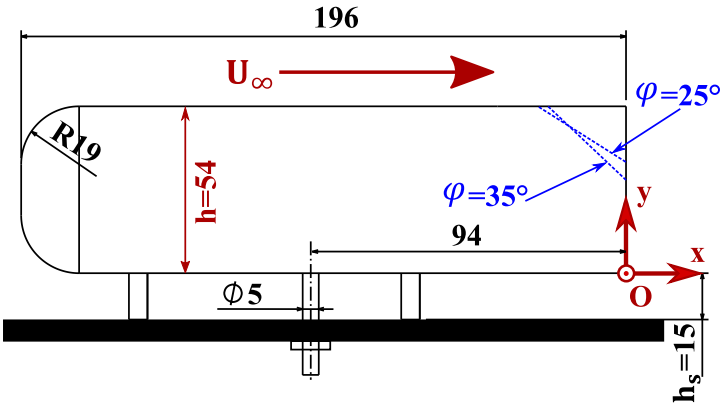

Figure 3: Side view of the models (Ahmed bodies at scale 0.19 with 0°, 25° and 35° rear slant angles) mounted on the floor of the test section. Dimensions are in millimetres. Flow direction and co-ordinate system are shown

Velocity measurements were recorded with a 2D LDV system manufactured by DANTEC Dynamics (model 2D Flow Explorer). In terms of optical properties, the two pairs of LASER beams have wavelengths of 660nm and 785nm. The fringe spacing were $5.45\mu m$ and $6.40\mu m$ in the longitudinal and vertical directions, respectively. The diameter and length of the measuring volume (in z-direction) are $168\mu m$ and 2.81mm respectively for the first component and $200\mu m$ and 3.34mm for the second component. The focal length is 500mm and Bragg cell frequency shifting is 80MHz. The LDV displacement in the plane (x, y) is controlled by a 2D traverse system. The LDV and traverse system are controlled by computer (BSA Flow Software, v5.03.00). The fog fluid used in this study is the SAFEX Inside Nebelfluid Extra Clean (provided by DANTEC), a mixture of diethylene glycol $C_4H_{10}O_3$ and water. The fog generator is the SAFEX S 195 G with adjustable flow rate. Generated particles have a mean diameter of $1.068\mu m$. Algieri et al. [11] recommended this seeding system for LDV measurements in air flows.

A photograph of the experimental set-up is given in Figure 4. In addition to all the instrumentation, the cylindrical rod that enables to fix the model on the floor can be seen.

For each of the three models, velocity measurements have been done in the wake flow region corresponding to $0.09 < X < 5.65$, $0 < Y < 1.3$. Four planes $Z = 0$, $Z = -0.23$, $Z = -0.45$ and $Z = -0.68$ have also been considered. Regarding models with $\varphi = 25°$ and $\varphi = 35°$, measurements on the rear slant have also been done. Due to interference with the ground, only 1D measurements have been done in the region $-0.28 < Y < 0.09$. When measurements have to be done close to the ground, the traverse system was inclined at 4.1°. Since its inclination is less than 5°, no correction on the results are needed (Tachie [12]). For 2D measurements, data acquisition lasts 90s at each location point in

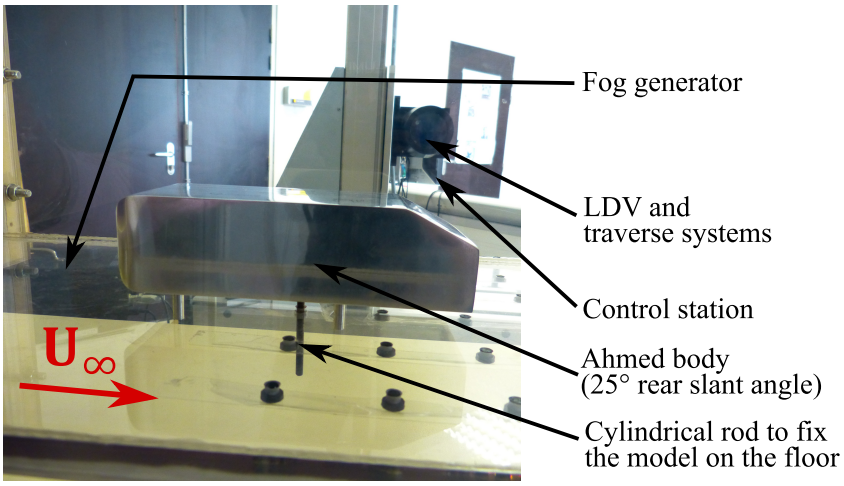

Figure 4: Photo of the instrumentation and experimental set-up with 25° rear slant Ahmed body

agreement with the calibration study. For 1D measurement and due to a finer spatial mesh, acquisitions have been recorded over a period of 10s.

3.2 Acquisition configuration and data treatment method to avoid flow statistic bias

Data were acquired with Individual Realization acquisition mode, named as "Burst mode" in BSA flow software. This means that data are stored each time a particle cross the measurement volume. Since estimation of Reynolds stresses $\overline{u'v'}$ requires that u and v are collected at the same time, the time coincidence condition is active : u and v are saved when both components are recorded at the same time. Furthermore, measurements of u and v must correspond to the same particle. Hence, measurements for which $\tau_i > \Delta t_{i+1} = t_{i+1} - t_i$ are not taken into account for further processing (Tropea et al. [13]). So, values that may correspond to the presence of multiple particles in the measurement volume are then avoided as expected by Nobach [14].

In this paper, only flow statistics are expected. Then, if we consider LDV measurements at a well-defined position for which N data (corresponding to N seeding particles) are collected during T seconds (acquisition duration), first and second order moments may be assessed as follow :

$$\bar{u} = \frac{\sum_{i=1}^{N} u_i g_i}{\sum_{i=1}^{N} g_i} \tag{1}$$

$$u' = \sqrt{\frac{\sum_{i=1}^{N} (u_i - \bar{u})^2 g_i}{\sum_{i=1}^{N} g_i}} \tag{2}$$

$$\overline{u'v'} = \sqrt{\frac{\sum_{i=1}^{N} (u_i - \bar{u})(v_i - \bar{v}) g_i}{\sum_{i=1}^{N} g_i}} \tag{3}$$

Where g_i is a weighting factor.

If we assume that time average value is equal to the arithmetic average of all realizations, then we consider $g_i = 1$. However, in case of Homogeneous Seeding (HS) condition (homogeneous spatial

distribution of seeding particles), McLaughlin and Tiederman [15] pointed out the correlation between the particle arrival rate and the instantaneous velocity. When the absolute instantaneous velocity is higher than the absolute time averaged velocity, more volume of fluid will pass throughout the probe volume. Then, more particles will across the measurement volume and so more high-velocity samples will be recorded. The opposite phenomenon occurs when absolute instantaneous velocity is lower than the absolute time averaged velocity. As a result, statistics calculated as an arithmetic average are skewed.

Since the transit time in the measuring volume is inversely proportional to the velocity, Buchhave et al. [16] proposed the transit time as weighting factor, that is $g_i = \tau_i$. Considering the 3D nature of the flow as well as the probe volume shape, this solution is mostly recommended in HS condition. Nevertheless, our experimental results showed that results in Non Homogeneous Seeding (NHS) condition differ from results in HS condition, so that repeatability is not guaranteed if this method is applied.

Hoesel and Rodi [17] proposed the interarrival time as weighting, that is $g_i = \Delta t_i = t_i - t_{i-1}$. Our experimental results showed that even if statistics are repeatable whatever the seeding conditions are, the systematic error described previously is not corrected.

Having an homogeneous seeding for a long time is known as a hard challenge in open wind tunnel, mainly in certain regions for recirculating flows, near stagnation points, in presence of vortices or in the close wake of a bluff body. Maintaining sufficiently high data rate is often ensured through bursts of particles meaning that a large amount of particles is sent into the flow within a relatively very short period. This lead to NHS condition with possible bias in data analysis due to burst effects. Being aware of the systematic error and burst effect in NHS condition, a new treatment method has been developed based on a new weighting factor, that is $g_i = \Delta t_i.\tau_i$. Proofs of accuracy and reliability according to the systematic error and burst effects are not developed in the present paper but a journal publication dealing with that specific topic will be submitted shortly. Nevertheless, this weighting factor is used for all calculations in the present study and the collected results are compared to that obtained in previous studies.

4 Experimental results of wake flow properties

For conciseness, we only present mean streamwise velocity fields and streamwise turbulence intensity fields in the symmetry plane $Z = 0$ of the three models. Properties regarding the vertical component of the velocity, Reynolds stresses and turbulent kinetic energy in various planes will be showed during the oral presentation. Note that all experiments have been made in the same wind tunnel with constant inflow properties, same scaled model, experimental set-up and LDV system parameters making comparisons more accurate.

4.1 Mean velocity fields

Figure 5 depicts the mean streamwise velocity fields in the wake of the three Ahmed bodies in the symmetry plane ($Z = 0$). In flow regions where both velocity components have been recorded, the corresponding vectors are plotted indicating the flow direction.

Figure 5(a) refers to the results of the squareback Ahmed body configuration ($\varphi = 0°$). Arrows show the pair of counter rotating vortices as it was seen Figure 2(a). By defining the recirculation length L_r

as follow

$$L_r = \max_{\bar{u}(X)<0} (X) \tag{4}$$

we find $L_r = 1.38$. The difference is less than 5% with respect to study of Lahaye [5] who obtained $L_r = 1.45$ but in different experimental conditions (see Table 1).

Author	φ	$\mathcal{R}e_h$	$H_s = h_s/h$	Blockage ratio	L_r
Lahaye [5]	0°	5.3×10^5	0.25	9%	1.45
Present study		4.95×10^4	0.28	4.6%	1.38
Wang et al. [10]	25°	5.3×10^4	0.17	4.1%	0.67
Tunay et al. [18]		1.48×10^4	0.17	2.3%	0.54
Present study		4.95×10^4	0.28	4.6%	0.57
Wang et al. [10]	35°	5.3×10^4	0.17	4.1%	1.03
Tunay et al. [18]		1.48×10^4	0.17	2.3%	0.97
Present study		4.95×10^4	0.28	4.6%	1.05

Table 1: Comparison of the recirculation length L_r between authors according to the experimental conditions

Figure 5(b) refers to the results with the rear slant angle $\varphi = 25°$. Acknowledging that measurements are quite impossible in the close vicinity of the rear slant, the strong downwash effect seems to indicate that the flow is fully attached on the rear slant, which is in contradiction with Figure 2(b). However, this behaviour agrees with the results of Thacker [6] who showed that when the edge between the roof and the slant is rounded (that is not rigorously sharp in our case), the flow is fully attached on the slant. Regarding the recirculation length in the near wake, we find $L_r = 0.57$. As we can see in Table 1, this result is included between those found by Wang et al. [10] and Tunay et al. [18] in their experimental studies.

Figure 5(c) refers to the results with the rear slant angle $\varphi = 35°$. The flow is fully detached from the rear slant and then the recirculation length is higher. We find here $L_r = 1.05$ which is very close (2% higher) to $L_r = 1.03$ found by Wang et al. [10] at almost equal Reynolds number but with different ground clearance (Table 1).

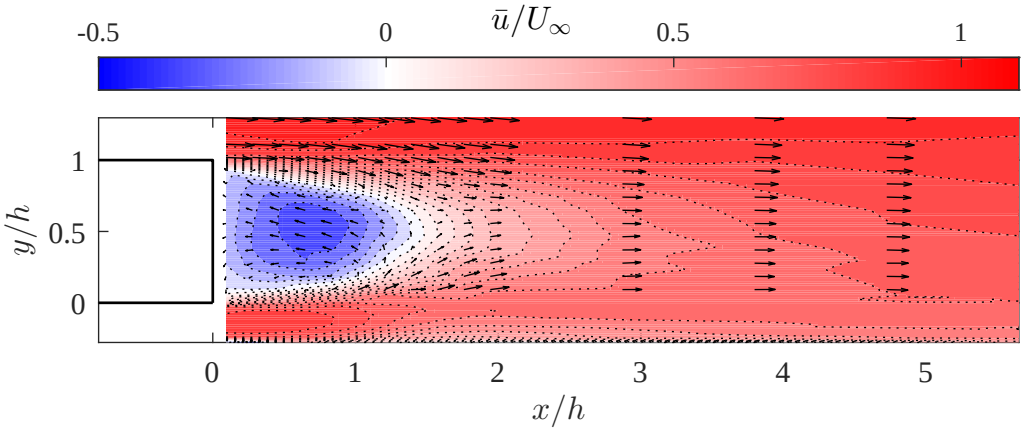

(a)

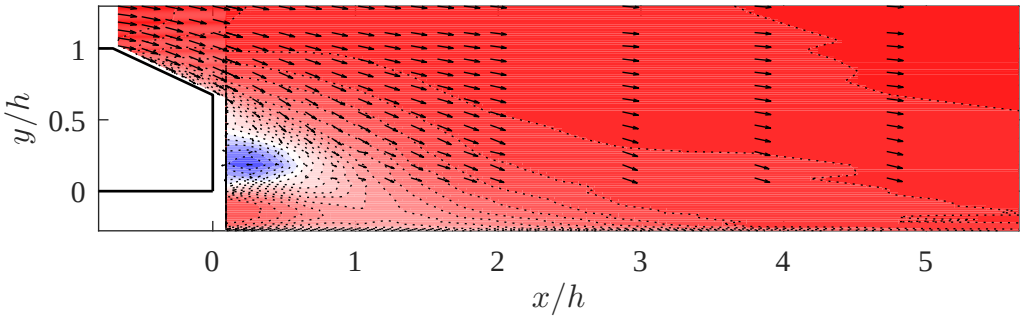

(b)

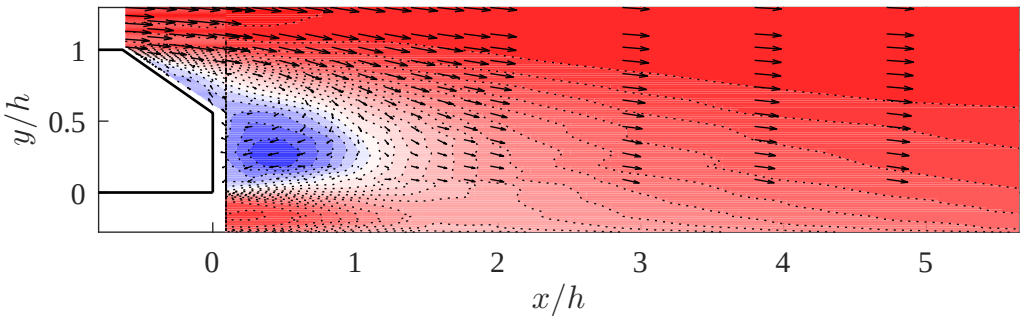

(c)

Figure 5: Mean streamwise velocity fields in the wake of the Ahmed bodies (arrows indicate flow direction with corresponding vectors) in the symmetry plane $Z = 0$: (a) $\varphi = 0°$, (b) $\varphi = 25°$, (c) $\varphi = 35°$

4.2 Turbulent fields

Figure 6 summarizes the streamwise turbulence intensity fields in the wake of the three Ahmed bodies in the symmetry plane ($Z = 0$). The meshgrid is also shown (black dots).

For the squareback configuration (Figure 6(a)), the maximum levels of turbulence intensity are located at the boundary of the recirculation region where velocity gradients are maximum. Maximum level of 27% is found at the dimensionless position $(0.90, 0.84, 0)$. Even out of the recirculation region where $X > L_r$, turbulence intensity is higher than 10%.

Due to the strong downwash effect for the configuration $\varphi = 25°$ (Figure 6(b)), region where turbulence intensity is higher than 10% is smaller than for the squareback configuration (Figure 6(a)), and it is located closer to the ground and the afterbody. Maximum turbulence intensity is about 27% and is located at $(0.43, 0, 0)$.

For $\varphi = 35°$ (Figure 6(c)), turbulence intensity in the upper shear-layer formed by the recirculating region on the rear slant and the upstream flow reaches 19% at $(-0.04, 0.93, 0)$. Downstream of the car model, the maximum intensity, reaching 29%, is located at $(0.65, -0.06, 0)$, in the shear layer formed by the flow coming from the underbody and the recirculation region. In the region where $X > 4$, turbulence intensity is less than 10%.

A comparative analysis on turbulent kinetic energy fields, defined as

$$K = \frac{1}{2U_\infty^2}\left(u'^2 + v'^2\right) \tag{5}$$

with the results of Tunay et al. [18] has been made for the configurations at $\varphi = 25°$ and $\varphi = 35°$ (see experimental conditions in Table 1). It shows that strong agreements are found in comparable regions between both studies having similar Reynolds numbers. For instance, similar maximum $K_{max} = 0.06$ has been measured in the regions:

- $Y \approx 0$ and $0.3 < X < 0.6$ for the configuration at $\varphi = 25°$
- $Y \approx 0$ and $0.7 < X < 1$ for the configuration at $\varphi = 35°$

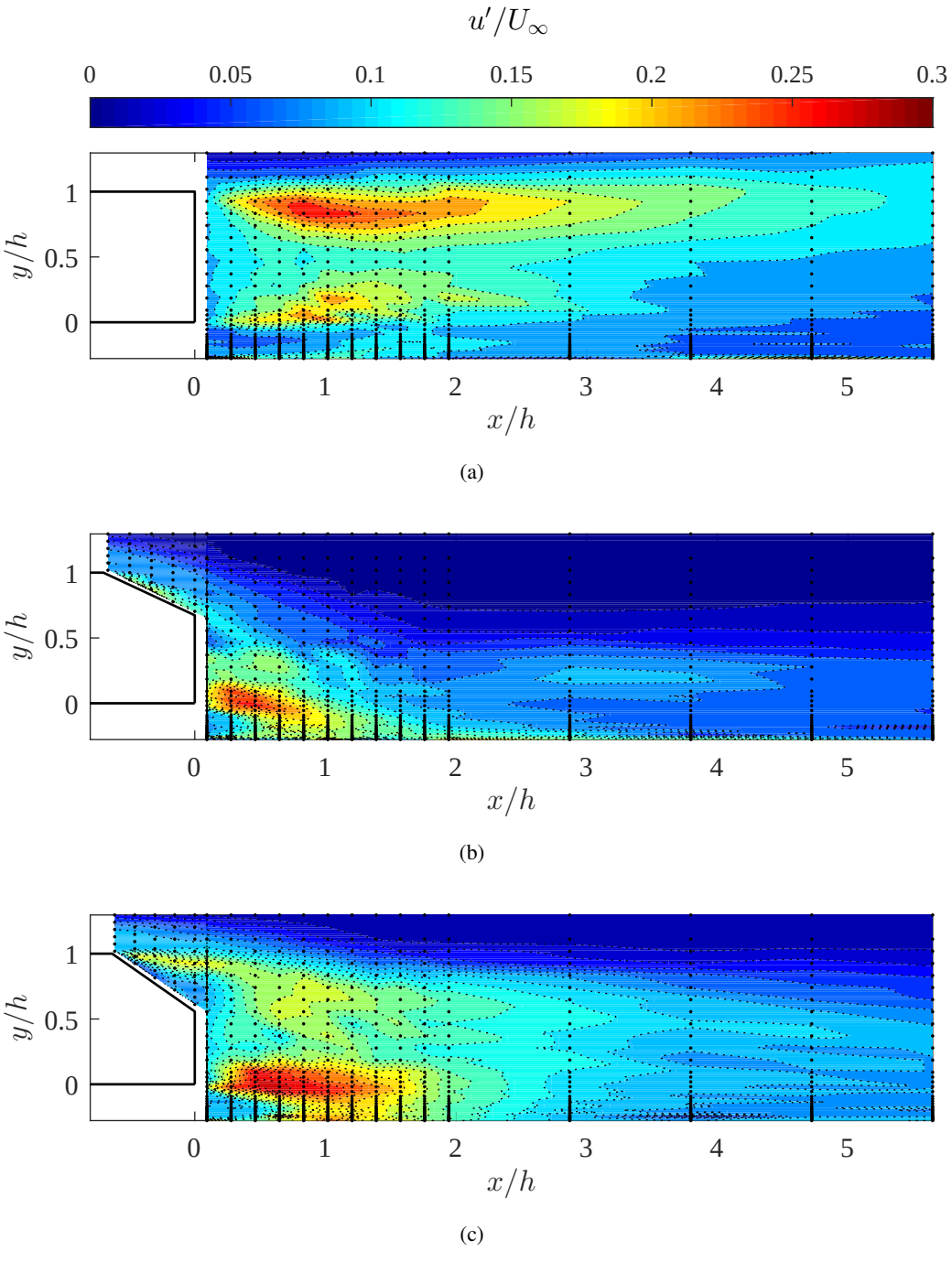

Figure 6: Streamwise turbulence intensity fields in the wake of the Ahmed (points represent the mesh-grid) in the symmetry plane $Z = 0$: (a) $\varphi = 0°$, (b) $\varphi = 25°$, (c) $\varphi = 35°$

5 Conclusion and further work

In this paper, it has been shown that our experimental investigations in the wake of three Ahmed bodies with the new data treatment method lead to results that are similar to those found by other authors. Note that in this paper, results taken from the literature have been obtained using another measuring system (Particule Image Velocimetry). The main advantage of our data treatment method deals with the fact that results are not dependent on the seeding conditions, which is hard to control in LDV measurements.

Nevertheless, these results have to be completed with other properties such as the counter rotating vortices and longitudinal vortices (Figure 2) positions, centers and volumes. Considering the goal of our research project, these investigations have to be correlated with particle number concentration (PNC) fields to discuss the interaction between turbulent vortical structures and nanoparticle distribution. The PALAS DNP 2000 system will be used for the nanoparticle generation (carbon particles with size ranging from 20 nm to 100nm) and the ELPI (Electrical Low Pressure Impactor) granulometer for PNC measurements. The recorded PNC fields in the wake of our models will then be assessed and compared to flow properties. The influence of the exhaust pipe on the flow properties will also have to be characterized. Finally, the interaction between two vehicles will be studied to evaluate the influence of the upstream one in terms of nanoparticles dispersion and penetration into the downstream one through air inlets. It is believed that altogether these results will be helpful to identify key parameters that influence particle path and possible infiltration in the following vehicle through air entrances.

Acknowledgment

The financial support of Regional Council of Pays de la Loire (France) and ESTACA is greatly acknowledged.

References

[1] A. Goel and P. Kumar, "Characterisation of nanoparticle emissions and exposure at traffic intersections through fast-response mobile and sequential measurements," *Atmospheric Environment*, vol. 107, pp. 374–390, 2015.

[2] P. Kumar, A. Garmory, M. Ketzel, R. Berkowicz, and R. Britter, "Comparative study of measured and modelled number concentrations of nanoparticles in an urban street canyon," *Atmospheric Environment*, vol. 43, no. 4, pp. 949–958, 2009.

[3] W.-H. Hucho, *Aerodynamics of road vehicles*. SAE, fourth edition ed., 1998.

[4] S. Ahmed, G. Ramm, and G. Faltin, "Some Salient Features Of The Time-Averaged Ground Vehicle Wake," *SAE Technical Paper Series*, feb 1984.

[5] A. Lahaye, *Characterization of the flow around a square back Ahmed body (in French)*. PhD thesis, Université d'Orléans (France), 2014.

[6] A. Thacker, *Experimental contribution to the steady and unsteady analysis of the flow behind a bluff body (in French)*. PhD thesis, Université d'Orléans (France), 2010.

[7] D. Barros, *Wake and drag manipulation of a bluff body using fluidic forcing*. PhD thesis, ISAE-ENSMA (France), 2015.

[8] A. Spohn and P. Gilliéron, "Flow separations generated by a simplified geometry of an automotive vehicle," in *IUTAM Symposium: unsteady separated flows*, (Toulouse, France), 2002.

[9] M. Grandemange, *Analysis and control of three-dimensional turbulent wakes: from axisymmetric bodies to road vehicles*. PhD thesis, ENSTA ParisTech (France), 2013.

[10] X. W. Wang, Y. Zhou, Y. F. Pin, and T. L. Chan, "Turbulent near wake of an Ahmed vehicle model," *Experiments in Fluids*, vol. 54, no. 4, 2013.

[11] A. Algieri, S. Bova, and C. De Bartolo, "Experimental and Numerical Investigation on the Effects of the Seeding Properties on LDA Measurements," *Journal of Fluids Engineering*, vol. 127, no. 3, p. 514, 2005.

[12] M. F. Tachie, *Open channel turbulent boundary layers and wall jets on rough surfaces*. PhD thesis, University of Saskatchewan (Canada), 2000.

[13] C. Tropea, A. L. Yarin, and J. F. Foss, *Springer handbook of experimental fluid mechanics*, vol. 53. 2007.

[14] H. Nobach, "Processing of stochastic sampled data in laser Doppler anemometry," in *Proc. 3rd Int. Workshop on Sampling Theory and Applications*, pp. 149–154, 1999.

[15] D. K. McLaughlin and G. Tiederman, William, "Biasing correction for individual realization of laser anemometer measurements in turbulent flows," *Physics of Fluids*, vol. 16, pp. 2082–2088, 1973.

[16] P. Buchhave, W. K. George, and J. L. Lumley, "The Measurement of Turbulence with the Laser-Doppler Anemometer," *Annual Review of Fluid Mechanics*, vol. 11, pp. 443–503, jan 1979.

[17] W. Hoesel and W. Rodi, "New biasing elimination method for laser-Doppler velocimeter counter processing," *Review of Scientific Instruments*, vol. 48, no. 7, pp. 910–919, 1977.

[18] T. Tunay, B. Sahin, and V. Ozbolat, "Effects of rear slant angles on the flow characteristics of Ahmed body," *Experimental Thermal and Fluid Science*, vol. 57, pp. 165–176, 2014.